Geomorphology 311 (2018) 37–50

Contents lists available at ScienceDirect

Geomorphology

journal homepage: www.elsevier.com/locate/geomorph

Quaternary landscape evolution of the Helmand Basin, Afghanistan: Insights from staircase terraces, deltas, and paleoshorelines using high-resolution remote sensing analysis

L.A. Evenstar *, R.S.J. Sparks, F.J. Cooper, M.N. Lawton

School of Earth Sciences, University of Bristol, UK

ARTICLE INFO

Article history:
Received 9 October 2017
Received in revised form 21 March 2018
Accepted 21 March 2018
Available online 23 March 2018

Keywords:
Afghanistan
Helmand Basin
Remote sensing
Geomorphology
Fluvial longitudinal profiles
Quaternary
Paleoenvironment
Landscape evolution

ABSTRACT

The Helmand Basin in southern Afghanistan is a large (310,000 km^2), structurally controlled, endorheically drained basin with a hyperarid climate. The basin hosts a high elevation (~200 m) plateau (the Dasht-i Margo), 11 fluvial staircase terraces (T11 to T1), 7 delta systems (D1 to D7), and 6 paleolake shorelines (SL1 to SL6) within the Sistan Depression on the western side of the basin. Mapping and surveying of these features by remote sensing is integrated with geological observations to reconstruct Quaternary landscape evolution of the basin. The fluvial systems, deltas, and paleolake shorelines are correlated with one another and with the younger terraces (T7 to T1). The shape of fluvial longitudinal profiles changes depending on whether they formed pre-, syn-, or post-growth of the Koh-i Khannesin volcano on the southern margin of the Helmand River. The age of the volcano (~0.6 Ma) and correlation of the terraces with the global history of glacial-interglacial cycles constrain the age of the younger terraces to the late Pleistocene and indicates that the older terraces are middle Pleistocene (dating back to 800 ka). The Helmand Basin once hosted a large lake, called here the Sistan paleolake, which at SL6 times and before had a surface area >50,000 km^2. Since that time the lake elevation and area have decreased, evolving to the present-day dried out Sistan Depression with small ephemeral playa lakes. Episodic formation of terraces, deltas, and paleolake shorelines is attributed to changes in base level modulated by climate change related to Milankovitch cycles.

Crown Copyright © 2018 Published by Elsevier B.V. All rights reserved.

1. Introduction

The majority of landscape development is based on reconstructions from a single geomorphic surface, e.g., fluvial terrace (e.g., Lavé and Avouac, 2000; Demir et al., 2004; Bridgland et al., 2012; Stokes et al., 2017), deltas (Horton and DeCelles, 2001; Hartley et al., 2010; Syvitski et al., 2012), or paleoshorelines (Currey, 1990; DeVogel et al., 2004; Drake and Bristow, 2006; Garcin et al., 2012). Within the Helmand Basin, the exceptional preservation of a large-scale plateau, staircase terraces, deltas and paleoshorelines allow these surfaces not just to be mapped and characterised individually but also to be linked into current and former longitudinal fluvial profiles over a basin scale. These studies enable an assessment of how landscape has responded to climate and tectonic processes within the Quaternary period.

The large scale of these surfaces and the hostile location lends itself to using remote sensing for analysis. With the increase in freely available satellite remote sensing data of Earth's surface, studies investigating geology and geomorphology in areas where field work can be difficult have seen an upsurge (e.g., the high Himalaya: Cooper et al., 2012; or the Pakistan/Afghanistan border: Ul-Hadi et al., 2013). Numerous studies looking at large-scale geomorphic features have exploited the use of remote sensing, for example in mapping fluvial terraces (Bridgland et al., 2012; Stokes et al., 2012), megalakes (e.g., Drake and Bristow, 2006; Garcin et al., 2012; Bachofer et al., 2014; Perkins et al., 2016), and deltas (e.g., Horton and DeCelles, 2001; Hartley et al., 2010). In this study we combine a number of different remotely sensed data sets to reconstruct the Quaternary evolution of the landscape within an area that has received little geological research since the 1970s (e.g., Pias, 1972, 1976; Smith, 1974).

The Helmand Basin is a large (310,000 km^2), structurally controlled, endorheically drained basin situated in a region with a hyperarid climate (precipitation < 100 mm/y). It is primarily fed by the Helmand River, which drains the Hazarajat Mountains and flows west into the Sistan Depression on the western edge of the basin (Fig. 1). Despite the hyperarid climate, the Sistan Depression contains numerous shallow lakes fed by the Helmand River, which host important agricultural and wetland areas with a long history of human habitation over at least the last 5000 years (Whitney, 2006; Lu et al., 2009). However, fluctuations in climate over the past century have led to regional droughts and conflict with neighbouring countries (Whitney, 2006). The communities of the Helmand Basin have relied heavily on sparse

* Corresponding author.
E-mail address: l.evenstar@bristol.ac.uk (L.A. Evenstar).

https://doi.org/10.1016/j.geomorph.2018.03.018
0169-555X/Crown Copyright © 2018 Published by Elsevier B.V. All rights reserved.

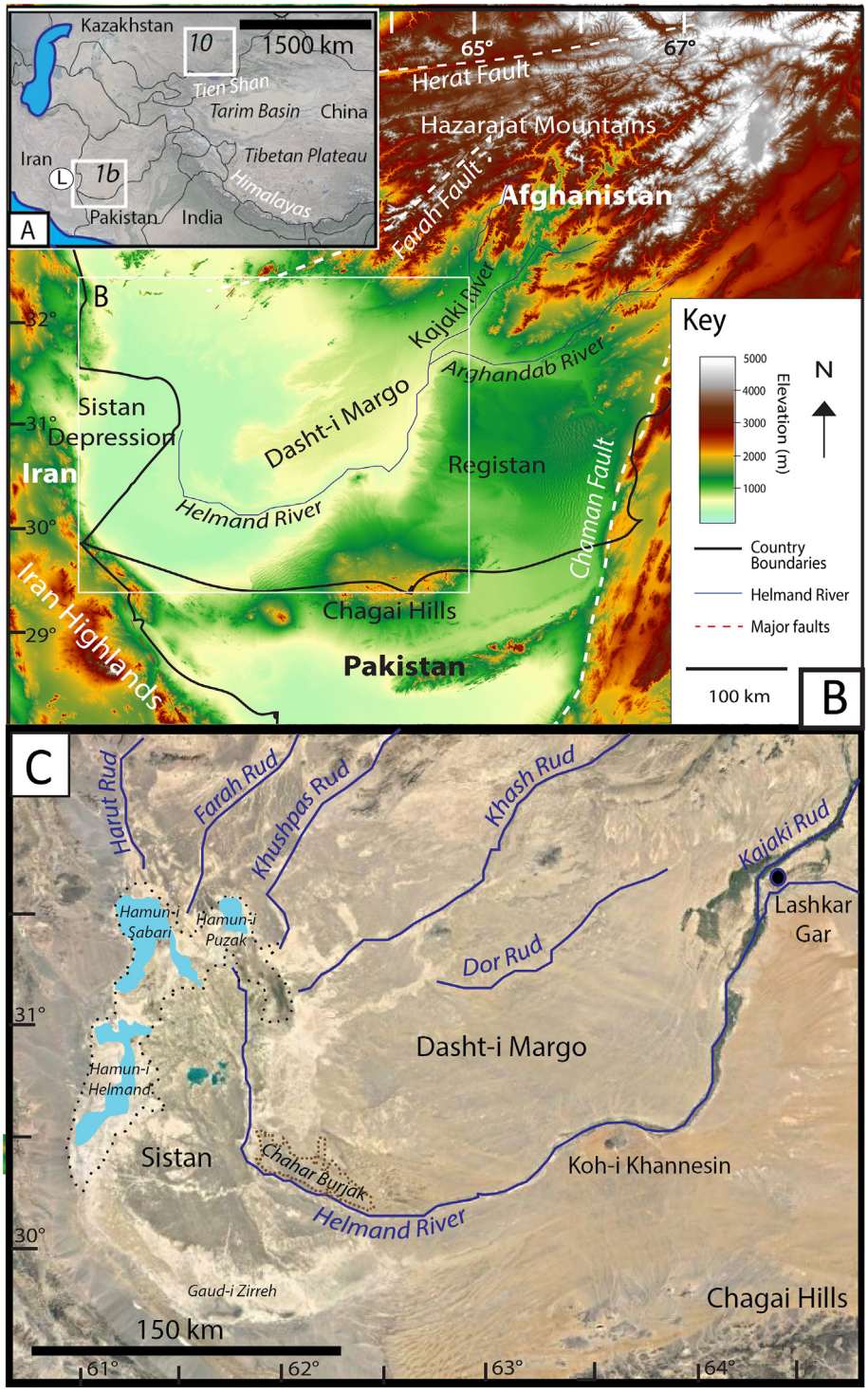

Fig. 1. (A) Regional Google Earth image of the Himalayan-Tibetan region with locations of figs. 1b and 10 denoted by white boxes, white circle L = Lut Desert in eastern Iran. (B) Digital elevation model of the Helmand Basin showing the main geomorphic regions and large-scale faults. (C) Google Earth image of the Helmand Basin showing the main rivers that flow into the basin and the playa lakes.

water supplies for drinking, irrigation, and energy production. This study places new constraints on how the landscape of the Helmand Basin has reacted to past climate fluctuations, which could be used to predict how this region could react to future climate change.

2. Physical geography of the Helmand Basin

The Helmand Basin dominates the southern part of Afghanistan and extends into eastern Iran and western Pakistan. The region is structurally enclosed, bordered on four sides by mountain ranges. The Hazarajat Mountains, part of the Karakoram-Himalayan mountain chain, form the northern border of the Helmand region and are the main source of sediments deposited in the basin (Fig. 1B) (Whitney, 2006). To the south, the Chagai Hills border the basin. In the west, the basin is bordered by the eastern Iranian highlands (Fig. 1B). The eastern margin of the basin is defined by the edge of the Registan Plateau rising up abruptly to the east of the Helmand River.

The Helmand Basin is fed by six main rivers sourced in the Hazarajat Mountains and flowing NE to SW into the Helmand Basin. These are from NW to SE: Harut Rud, Farah Rud, Khaspas Rud, Khash Rud Dor Rud, and Helmand Rud (Fig. 1C). The Helmand is the largest river and contributes over 80% of discharge into the basin. The Helmand River runs NE to SW and separates the Dasht-i Margo in the north from the Registan Desert in the south, terminating in the Sistan Depression in the west. Most discharge (90%) occurs between February and June from snowmelt and spring precipitation in the Hazarajat Mountains (Whitney, 2006). Discharge of the Helmand River has a long-term mean discharge of 9500 Mm^3/y (1952–2012), but discharge fluctuates markedly from year to year with successive years of drought (Goes et al., 2016).

The climate of the region is hyperarid with precipitation rates <100 mm/y. Some of the highest evaporation rates in the world have been recorded in the lower Helmand Basin (Warsaw, 1984; Whitney, 2006). Temperatures can exceed 50 °C in summer and occasionally drop to below 0 °C in winter (Warsaw, 1984; Whitney, 2006). The desert winds, called the bad-i-sad-o-bist Ruz (*winds of 120 days*), often reach hurricane force (100–130 kph) and are common from May until September (Whitney, 2006). They are a major erosional agent and have formed widespread yardangs across the lower Helmand Basin (McCauley et al., 1977; Ranjbar and Iranmanesh, 2008). The winds blow from the northwest and are funnelled between the Afghanistan and Iranian mountains along the western edge of the basin. Toward the southern edge of the basin, the winds are deflected to the east by the Chagai Hills (Fig. 2).

The Helmand Basin can be divided into five geomorphological regions: the Sistan Depression the Dasht-i Margo Plateau, the Registan Desert, the Hazarajat Mountains, and the Helmand River itself (Fig. 1B).

The Sistan Depression (Fig. 1B) forms the lowest part of the Helmand region with an area of 18,000 km^2 and minimum elevation of ~425 m asl. The western and southern edges of the depression are characterised by a series of ~10- to 50-km-long alluvial fans that originate from the Iranian mountains and terminate in extensive wetlands and three playa lakes. The playa lakes, called hamuns (Hamun-i Puzak, Hamun-i Sabari, and Hamun-i Helmand), usually have depths of <3 m, but during times of high discharge from the Helmand River merge to form a single lake and overspill to the south into the Gaud-i Zirreh (Whitney, 2006). During periods of drought the playas can completely dry up. Along the eastern edge of the Sistan Depression several deltas (termed distributary fluvial systems) have been recognized that terminate in the playa lakes (Hartley et al., 2010). The largest of these delta systems originates from the Helmand River.

To the east, the Dasht-i Margo (*Desert of Death*) forms a high plateau, ~300 m above the Sistan Depression. It covers an area of 15,000 km^2 across much of the northeastern part of the Helmand Basin. The plateau is a gently inclined surface that ranges in height from ~900 m at the foothills of the Hazarajat Mountains to ~730 m adjacent to the Sistan Depression. The northeastern side of the Dasht-i Margo Plateau is marked by a faulted ridge of early Cretaceous limestones and sandstones, which has been deeply incised by the Khash Rud River (Fig. 1C). The southwestern side of the plateau is incised by the Helmand River. The Dasht-i Margo marks the top of the sedimentary fill of the Helmand Basin (Whitney, 2006).

To the northeast of the Dasht-i Margo, the Hazarajat Mountains rise up forming the highest mountains in Afghanistan with a maximum elevation of 7078 m. The region is still seismically active, suggesting ongoing uplift (Ruleman et al., 2007).

The Helmand River flows for over 1300 km terminating in the Sistan Depression. It enters the Helmand Basin along its northeast margin where it is joined by the Arghandab River near Lashkar Gar (Fig. 1B). The river curves around the northeast side of Koh-i Khannesin, a carbonatite volcano dated at 0.61 ± 0.05 Ma by K-Ar dating of a leucite phonolite (unpublished age by Richard Marvin, U.S. Geological Survey, written commun., 1977, cited in Whitney, 2006) (Fig. 1C). On entering the Sistan Depression the river changes direction and flows to the north terminating in a delta system into the Hamun-i Pazak playa lake (Fig. 1C). The river cuts into the Dasht-i Margo plateau by up to 180 m and averages 2 km in width. Two prominent terraces have been documented along the entire extent of the river. Within the upper reaches between Koh-i Khannesin volcano and Lashkar Gah, the river

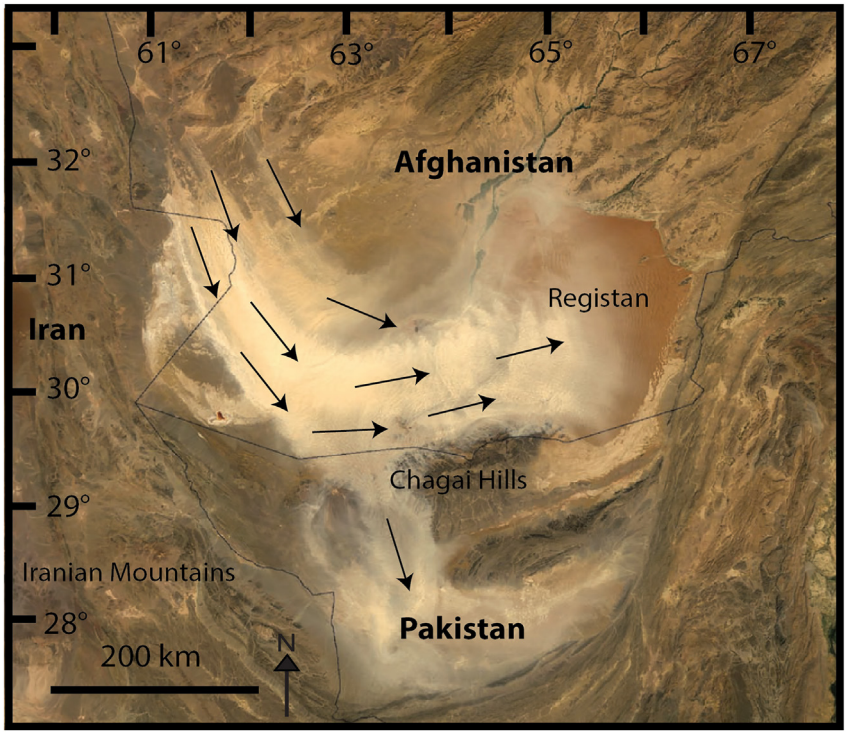

Fig. 2. Moderate Resolution Imaging Spectroradiometer (MODIS) image of the Helmand Basin taken on 13 September 2003 (Whitney, 2006). White dust and arrows highlight the prevailing wind direction and deflection of the winds first southward along the edge of the Iranian Mountains and then eastward along the edge of the Chagai Hills.

is wider and four terraces have been recognized (Whitney, 2006). As the Helmand River enters the Sistan Depression, a ~610-m high plateau (>400 km^2) is located to the north of the river and recorded as an older distributary fluvial system termed the Chahar Burjak (Fig. 1C).

The southeastern part of the Helmand Basin is dominated by the Registan plateau (*Land of Sand*) that hosts a 25,000 km^2 inactive sand sea with an average elevation of 1000 m asl that increases in elevation by 200 m toward the northeast edge of the basin (Fig. 1B). Along the western edge of the Registan, linear dunes form parallel to the wind direction partially overlying late Pliocene fluvial conglomerates and sandstones (Doebrich et al., 2006). Toward the eastern edge of the Registan region the dunes form regionally extensive barchanoid sand dunes. Inactive red dunes up to 75 m high with parasitic active white-tan dunes migrating over them dominate the region.

3. Geological setting

3.1. Tectonic and volcanic history

The Helmand Basin formation reflects a long tectonic history of interactions between continental plates and microplates (Shiel, 2017). The Helmand Basin lies within the Afghan microplate, formed from the collision of several microplates in the Mesozoic (Whitney, 2006; Shiel, 2017). In the early Cretaceous, the Afghan microplate collided with the Eurasian plate, forming the northern margin of the basin marked by the Hazarajat Mountains. Within the Eocene, the Indian plate collided with the Eurasian plate and converged westward against the Afghan plate (Aitchison et al., 2007; Shiel, 2017). With increased crustal shortening the Hindu Kush Mountains formed, and the Afghan plate was forced to the southwest along a series of wrench faults (Whitney, 2006). The two most important microplate-bounding faults are the 1100-km long Herat fault within the Hazarajat Mountains (Wheeler et al., 2005) and the 800-km long Chaman fault on the eastern edge of the Afghan plate (Fig. 1B). Both faults show active displacement rates of 0.4 mm/y and 33.3 ± 0.3 mm/y respectively (Wheeler et al., 2005; Ul-Hadi et al., 2013). A number of smaller faults with a similar strike to the Herat and Chaman faults are recognized across the basin but have lower estimated displacement rates (Ruleman et al., 2007). The fault systems bordering the Helmand Basin are still active (Wheeler et al., 2005; Whitney, 2006; Ruleman et al., 2007; Ul-Hadi et al., 2013; Fattahi and Amelung, 2016).

The eastern and southern margins of the Helmand Basin are related to the movements of the Arabian plate with the opening of the Red Sea (Reilinger and McClusky, 2011). The still seismically active eastern mountains of Iran that border Helmand Basin are related to the distributed deformation as the Arabian Shield moves NNE at about 3 cm/y. To the south of the basin, subduction of the Arabian plate sea floor has developed a wide zone of deformation (the Makran subduction zone). Opening of the Red Sea initiated about 24 ± 2 my (Reilinger and McClusky, 2011). Collision of the Arabian craton with the Eurasian plate to form the mountain barriers on the eastern and southern margins of the Helmand Basin started in the late Miocene.

In the late Eocene, volcanism formed the Chagai Hills along the southern boundary of the Helmand Basin (Perelló et al., 2008). In the Miocene, a number of volcanoes formed along the western edge of the Sistan Depression; the youngest being the Koh-i Chekab at 8.2 ± 6.0 Ma and an isolated basalt flow dated at 7.3 ± 2.0 Ma forming a mesa within the Hamun-e Helmand playa and placing age constraints on the younger sediments in the basin (Jux and Kempf, 1983).

3.2. Sedimentary history

Sediments provide a record of relief generation and drainage routing across the region. However, the sedimentary infill of the Helmand Basin is limited, with little work in the region since the 1970s (Pias, 1972, 1976; Wittekindt and Weippert, 1973; Smith, 1974; Quittmeyer and Jacob, 1979; Whitney, 2006). Aeromagnetic surveys suggest 3–5 km of sedimentary infill lie above the Precambrian basement in the Sistan region (Schreiber et al., 1972). Neogene and Quaternary sediments are estimated to be up to 1000 m thick with only the top 250 m exposed along the edge of the Helmand River (Whitney, 2006). The sediments are described as conglomerates, sandstones, and mudstones deposited by fluvial, aeolian, and lacustrine processes (Smith, 1974). The sequence is flat-lying except close to the borders of the Iranian and Pakistan mountain ranges where the deposits have minor southward or westward tilting respectively, suggesting minor tectonic movements (Jux and Kempf, 1983).

The exposed sequence along the edge of the Dasht-i Margo Plateau is divided into two units. A lower unit, the Sistan Beds (>250 m thick), consists of cross-bedded fluvial and aeolian sandstones with occasional lacustrine mudstones. The sediments fine toward the western edge of the Dasht-i Margo Plateau into predominantly laminated lacustrine mudstones, suggesting a large lake or several smaller lakes within the Sistan Depression in the past (Smith, 1974). The Sistan beds are the predominate sediments through which the later geomorphic features cut. This unit is overlain throughout the region by a flat-lying erosional disconformity covered by gravels and coarse sands with thickness varying from <1 to >15 m (Smith, 1974). These coarse deposits interfinger with alluvial fans along the edge of the basin toward the Hazarajat Mountains (Smith, 1974). Several gypsum and calcrete paleosols are present at the surface and at shallow depths of 15–30 cm (Smith, 1974; Doebrich et al., 2006). The age of the sediments in the Helmand Basin is poorly constrained. Along the Helmand River, lacustrine sediments overly volcanic units from the 0.61 Ma Koh-i- Khannesin volcano, supporting a late Pleistocene age for these sediments. Because the exposed sections here represent only a third of the total sediment thickness, the observations are consistent with sedimentation in the Miocene and Pliocene into the late Pleistocene.

Within the center of the Sistan Depression in Lake Hamun, a small mesa (~3 km^2) called the Kuh-i Khwaja (Fig. 3) is comprised of 55–60 m of lacustrine sediments capped by basalt (50 m) dated at 7.3 ± 2.0 Ma (Jux and Kempf, 1983). Within 3 km of the base of the mesa, two cores through lake sediments (<7 m) have a late Pleistocene age (Hamzeh et al., 2016). Together these data suggest that the Sistan Depression has experienced lacustrine conditions since, at the least, the late Miocene. However, the erosional remnant of the Kuh-i Khwaja mesa implies at least one cycle of lacustrine sedimentation, erosion, and then resedimentation.

Several studies proposed that the Sistan Depression hosted a large megalake in the Quaternary (>12,000 km^2), accounting for the widespread deposition of lacustrine sediments in the region (Huntington, 1905; Smith, 1974; Jux and Kempf, 1983; Whitney, 2006; Hamzeh et al., 2016). Huntington (1905) documented two former shorelines at 3 and 10 m above the playa lakes, which he interpreted as lake highstands in the late Pleistocene. He also inferred 10 pluvial to arid phases based on alternating oxic to anoxic lacustrine sediments. However, other studies proposed that the thick accumulations of lacustrine sediments are the consequence of long-lived subsidence of the Sistan Depression creating accommodation space for many smaller local lakes (Whitney, 2006). Smith (1974) suggested that the Sistan Depression hosted much larger volumes of sediments that have since been removed by aeolian erosion, an interpretation supported by remote sensing studies (Ranjbar and Iranmanesh, 2008). Within the Holocene, small-scale fluctuations of the climate between arid phases and humid phases are suggested from geochemical, sedimentological, and paleontological analysis of the Sistan Depression sediments (Hamzeh et al., 2016). Analysis suggested an increase in lake size from 6 to 3.8 ky, which correlates with the Bronze Age settlements and a decrease in lake size post-3.8 ky when these settlements were abandoned (Hamzeh et al., 2016). These changes suggest waxing and waning of the climate.

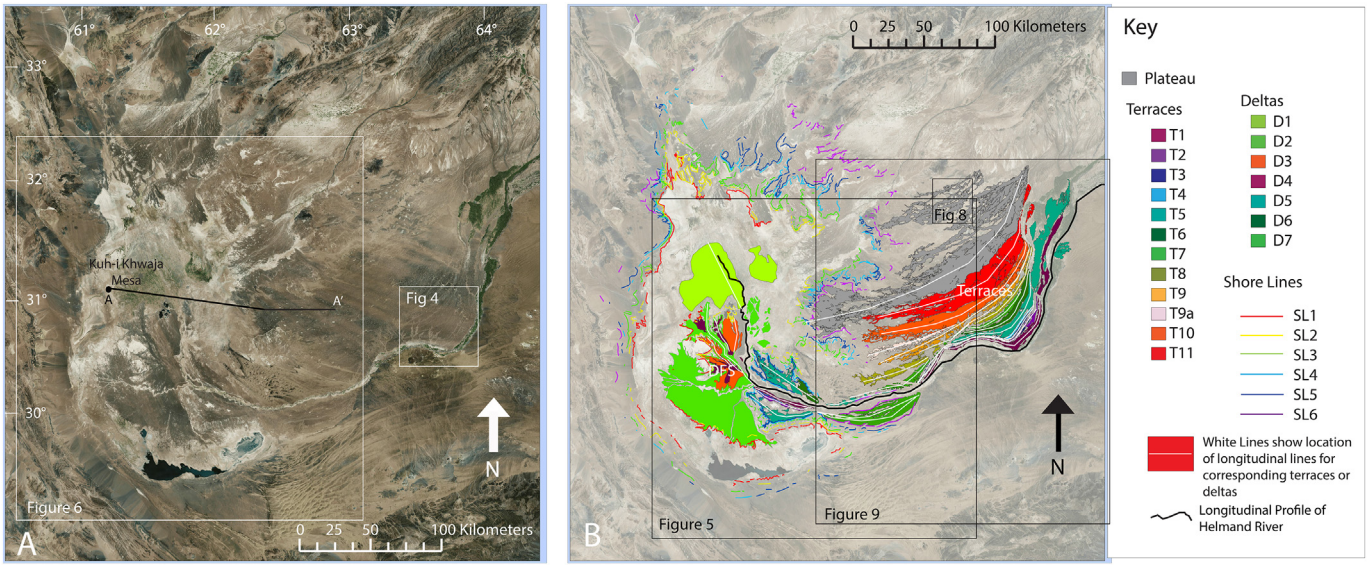

Fig. 3. TerraColor imagery of the Helmand Basin. (A) White boxes denote the locations of Figs. 4 and 6. (B) Mapped geomorphic surfaces (river terraces, deltas, and lake shore lines) are described in detail in the text. Black boxes denote the locations of Figs. 5, 8 and 9. Thin white lines along terraces show locations of longitudinal profiles.

3.3. Regional climate and its history

The Helmand Basin region is influenced by several atmospheric circulation patterns. To the north lies the Mid-Latitude Westerlies, which bring moisture from the Mediterranean controlling precipitation within the winter months and dominating the current hydroclimate in the Helmand Basin and its source regions within the Hazarajat Mountains (Benn and Owen, 1998; Owen and Dortch, 2014; Hamzeh et al., 2016). To the south lies the low-pressure cell of the Asian Summer Monsoon, which generates precipitation in the summer months (Benn and Owen, 1998; Owen and Dortch, 2014). Which of these systems is dominant depends on the strength of the high-pressure Siberian anticyclone, known as the Siberian High, to the north (Benn and Owen, 1998; Owen and Dortch, 2014; Hamzeh et al., 2016). When the Siberian High weakens there is increased influence of the Asian Summer Monsoon, and as it strengthens, more influence from the Mid-Latitude Westerlies (Hamzeh et al., 2016). The waxing and waning of the Siberian High has led climate variations within the Pleistocene to Holocene that are documented in geomorphic features to the west in Iran (Kehl, 2009, and reference within) and to the east in the western Himalayas and Pakistan (Owen and Dortch, 2014, and reference within).

How the intensity of the Siberian High changes between glacial to interglacial times and what affect this has on climate are not well understood (Kehl, 2009; Owen and Dortch, 2014). Within Iran the analysis of lake sediments, paleosols, and aeolian sediments suggest that during glacial periods the Siberian High strengthens and the conditions are dry and cold with intensification of dominantly northeasterly to northwesterly winds (Kehl, 2009). In interglacial periods, conditions are warmer and moister with increased evaporation that Kehl (2009) proposed led to paleosoil formation and development of saline lakes (Kehl, 2009). Through time these cycles have varied in strength with the lower to mid-Pleistocene hosting wetter conditions with deposition of a broad shallow lake in the now desert region of the Lut Basin in eastern Iran (Fig. 1A). Since that time, the Lut Basin has become drier with large volumes of lacustrine sediment removed from the basin and redeposited as giant yardangs in the Lut dune field (Bobek, 1969; Krinsley, 1970; Dresch, 1976).

To the west, the western Himalayas (the Hazarajat Mountains) supplies the Helmand River and is the major source of sediment supply for the basin. Here, Mid-Latitude Westerlies and northern hemisphere climate systems primarily control climate, while the rest of the Himalayas responds to variation in the Asian Summer Monsoon (Dortch et al., 2013). Geomorphology data from glacial landforms and fluvial terrace suggest that the glaciation in the western Himalaya broadly responds to Milankovich cycles (Owen and Dortch, 2014). During glacial periods the Siberian High is thought to strengthen, leading to increased glaciation in the western Himalayas (Owen and Dortch, 2014). In agreement with the findings in Iran, the western Himalayas became increasingly arid during the Quaternary (Owen et al., 1997).

4. Methods

The landforms are documented in this paper using remote sensing. The hyperarid conditions allow interpretation of the geomorphology from remote sensing data unhindered by vegetation. Doebrich et al. (2006) produced a digested map in ArcGIS and used this map for the purpose of documenting the regional geology, but not the geomorphology. Here we used and modified this map to show the regional geomorphology. The geomorphology of the Helmand Region was also characterised using a combination of the several remote sensing data sets covering an area 27–33°N to 60–66°E (a detailed description of the data set used can be found within Appendix 1):

- Global Digital Surface model data (1 arc sec) from the Japanese Advanced Land Observation Satellite (ALOS) with pixel size of 30 m and a height accuracy of 5 m. The ALOS comprises three sensors: the panachromatic stereo imager (PRISM) for optical measurement of land elevation, a visible and near infrared radiometer, and a phased array L-band synthetic Aperture Radar (PALSAR).
- Digital Elevation Data (1 arc sec Shuttle Radar Topography Mission (SRTM)-derived digital elevation data) from Advanced Spaceborne Thermal Emission and Reflection Radiometer (ASTER) satellite data with a horizontal accuracy of 30 m in most locations and up to ~10–25 m.
- Satellite and air imagery (VNIR – Visible Near-Infrared) images downloaded from ESRI. Small-scale images (~1:288 to ~1:72 k) were constructed from 2.5 m SPOT Imagery and larger scale images (~1:591 M down to ~1:72 k) from 15-m TerraColor imagery (based on the natural colour processing of Landsat 7 satellite).
- Landsat scenes from the Landsat 7 satellite using eight bands of multispectral scanning radiometer (radiation in near visible infrared (NVIR), shortwave infrared (SWIR), longwave infrared

(LWIR), and panachromatic bands from Earth's surface). Landsat images display band 7 (displayed in red), 4 (displayed in green), and 2 (displayed in blue). The Enhanced Thematic Mapper (ETM+) has a resolution of ~30 m.

A combination of all of these data sets were imported into ArcGIS and manipulated to highlight scenes that provide enough detail to identify, characterise, and map the key geomorphic elements manually: the Dasht-i Margo Plateau, fluvial terraces, delta systems, and shorelines within the Sistan Depression (Fig. 3). The ALOS data set, which has higher resolution elevation (~5 m) data, was used in combination with the SPOT imagery for high resolution mapping and recording the heights of small-scale features <10 km, such as shorelines, fluvial terraces, and channels on the Dasht-i Margo surface. The lower resolution elevation SRTM was used for large scale (>10 km) mapping of the terraces and deltas. However, the heights obtained from the SRTM-derived data sets also agreed well with the higher resolution data sets obtained from the ALOS.

Each of the landforms required a slightly different technique that will be described below. The upper surface of the Dasht-i Margo Plateau was examined on a large scale by the SRTM DEM data, LANDSAT, and TerraColor visual imagery. The individual channels had previously been mapped in Doebrich et al. (2006) as braided lobe calcretes. These channels were examined using the ALOS and SPOT visual imagery to estimate height and spatial distribution.

The fluvial terraces along the Helmand River were identified using standard procedures documented in Stokes et al. (2012) and references within. They were primarily identified using a shaded relief map of the area created with ALOS data that highlighted sharp changes in relief (Fig. 4). Terrace surfaces are light and smooth, while slope breaks between different terrace levels were darker and coarser. This approach was combined with a series of elevation profiles from the ALOS data perpendicular to the terraces to identify any breaks in slope (Fig. 4). The mapped terraces were also compared using the LANDSAT and SPOT visual imagery to check correlations. The elevations of the terraces were recorded from the modern river level and numbered from the base up, in elevation, which is common practice in previous fluvial terrace studies (e.g., Stokes et al., 2017). The terraces were then mapped using a combination of all remote sensing data (VNIR and SWIR, SRTM DEM, shaded relief) to investigate their spatial distribution. Over 100 elevation profiles were constructed using the STRM data across the region to assist with mapping and correlating the terraces. Correlating different terraces along a river can be a challenge (Stokes et al., 2012), and where the correlations are not certain, they are indicated by a dotted line. The correlations assume little influence from tectonics along the Helmand River, which is consistent with the flat-lying stratigraphy in the region and absence of visual faults within the remote sensing (Jux and Kempf, 1983). The spatial map was then used to construct a morphology-based landform stratigraphy.

Delta systems are characterised by their radial, distributary pattern with low slope values away from the main apex (Hartley et al., 2010). Because the systems change in elevation away from the apex, the authors had to use a technique that highlights the distributary pattern. In order to map the deltas originating from the Helmand River, we identified the lowest and highest point of all the delta systems (475 and 705 m). This approach was used to exclude elevations above and below this and created 23 contours of 10 m elevation with a colour spectrum from grey through red for each interval (Fig. 5A). This approach allowed us to highlight the radial distributary pattern and apex of each delta system. Using this and the sharp changes in relief between different delta systems, the authors mapped individual systems and their spatial distribution across the basin. The results were checked with the LANDSAT and SPOT visual imagery to confirm correlations (Fig. 5B).

Fluctuating lake levels within megalakes leave behind a variety of geological and geomorphic evidence (e.g., Currey, 1990; Atwood, 1994). These key lake evolution features are particularly clear at megalake level scale and can be recognized and mapped using remote sensing techniques (DeVogel et al., 2004; Drake and Bristow, 2006; Gaber et al., 2009; Bachofer et al., 2014). Within semiarid to hyperarid basins, shoreline deposits - such as beach wave-cut cliffs, gravel beach ridge and algal-carbonate (stromatolites or oncolites) beach ridges – can be used to identify former shorelines (Currey, 1990; Casanova and Hillaire-Marcel, 1992; Clapperton, 1993; DeVogel et al., 2004; Gaber et al., 2009; Bachofer et al., 2014). Within the Helmand Basin, a series of shorelines were identified from LANDSAT and TerraColor visual imagery on the larger scale and examined in detail on the SPOT imagery. In particular, white linear bands parallel to the playa level were identified as depositional beach ridges, most likely partly cemented by carbonate (Fig. 6). In other areas, the wave cut platforms can be recognized as beach ridges cutting into the alluvial fans along the edge of the basin (Fig. 6). To look at the elevation of the shoreline higher elevation ALOS data was used. By recording the elevations of the shorelines in regions where they are well preserved, we could then apply a threshold number to the SRTM DEM producing consistent shoreline heights to aid mapping across the entire basin (Fig. 6). The heights of the shorelines were recorded and traced around the basin. The correlations across the basin were checked with the LANDSAT, TerraColor, and SPOT visual imagery. The lower elevation shorelines showed more complete preservation than the higher elevation shorelines, which are frequently

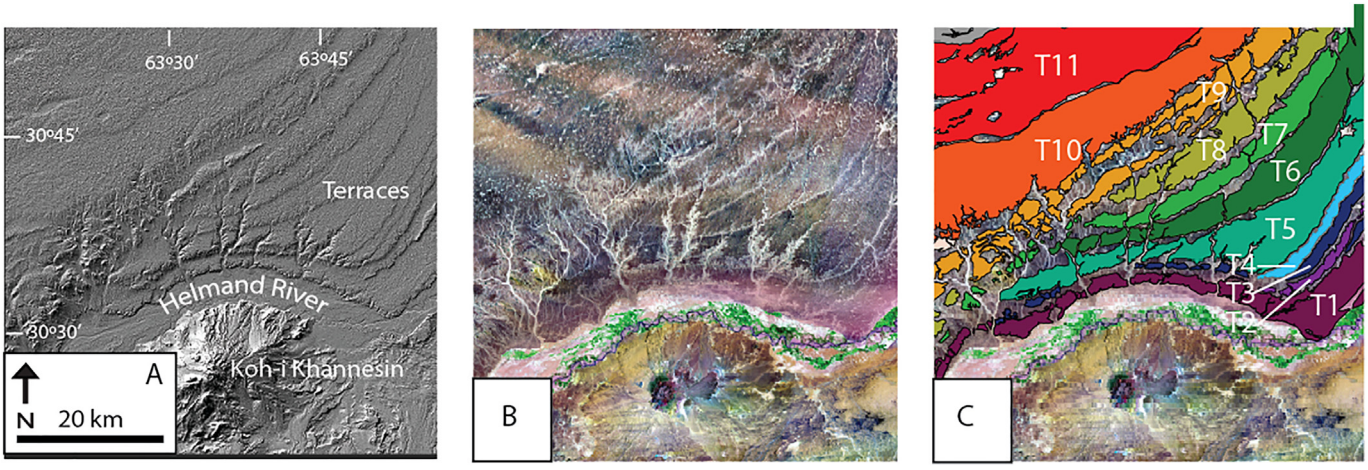

Fig. 4. (A) Shaded relief map constructed from Advanced Land Observation Satellite (ALOS) data of the Helmand River terraces around the Koh-i Khannesin volcano. Shadows highlight the sharp changes in relief used to map the terraces. (B) LANDSAT image of the same region showing similar colour and texture between terraces. (C) Mapped staircase terraces from sharp changes in relief highlights in A.

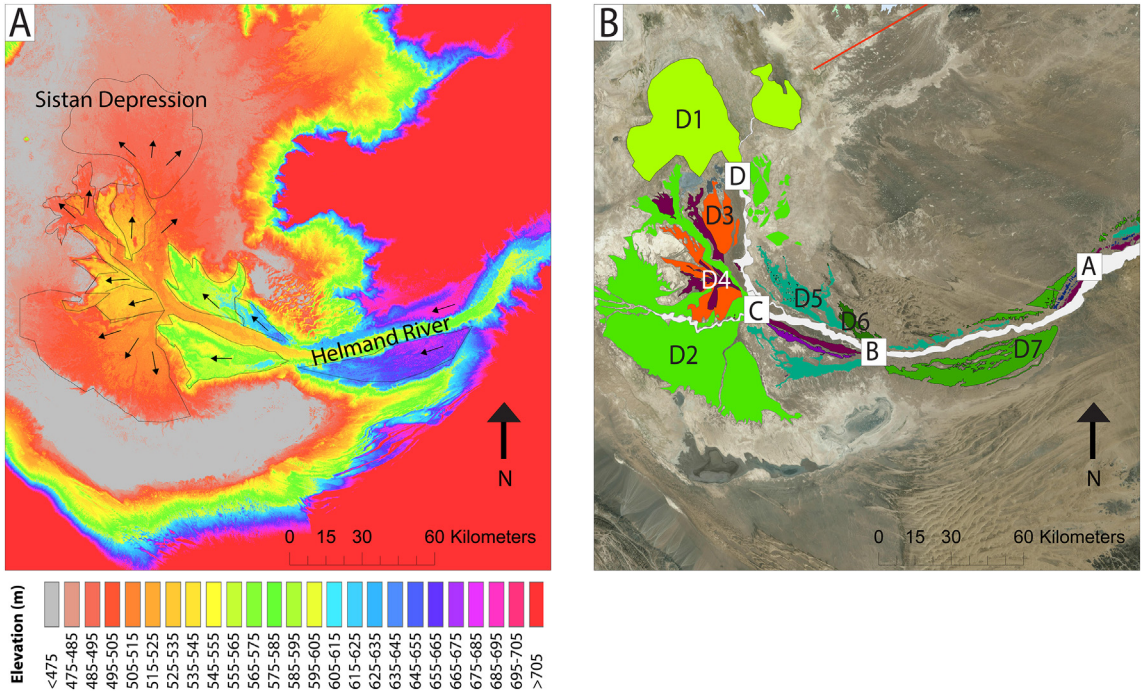

Fig. 5. Deltas originating from the Helmand River. (A) SRTM DEM data of elevations above and below 475 and 705 m are removed, and colour spectrums from grey through to red are stretched creating 23 contours of 10 m for each interval. The sharp changes in relief between the different delta systems are highlights by the sharp changes in the colour spectrum. The black lines outline the main deltas that are mapped in B and the black arrows highlight the radial distributary systems. (B) Mapped delta systems (D1–D7) in the Sistan Depression. Apexes of the deltas discussed in the text are labeled A–D and show telescoping out into the basin. (For interpretation of the references to colour in this figure legend, the reader is referred to the web version of this article.)

covered or incised by young fluvial or aeolian processes. The shorelines were predominantly correlated across the basin using height above the playa floor, which assumed no tectonics in the region consistent with the flat-lying sediments in the area.

The key geomorphic elements were manually digitized and the SRTM DEM scenes used to construct large-scale longitudinal profiles across the plateau, terraces, deltas, and modern Helmand River.

5. Observations

5.1. The Dasht-i Margo Plateau

The Dasht-i Margo forms an elevated plateau with an average slope of <0.034° to the southwest (Fig. 3). The area from the edge of the Sistan Depression to Lashkar Gah shows a lower slope of 0.015°, which

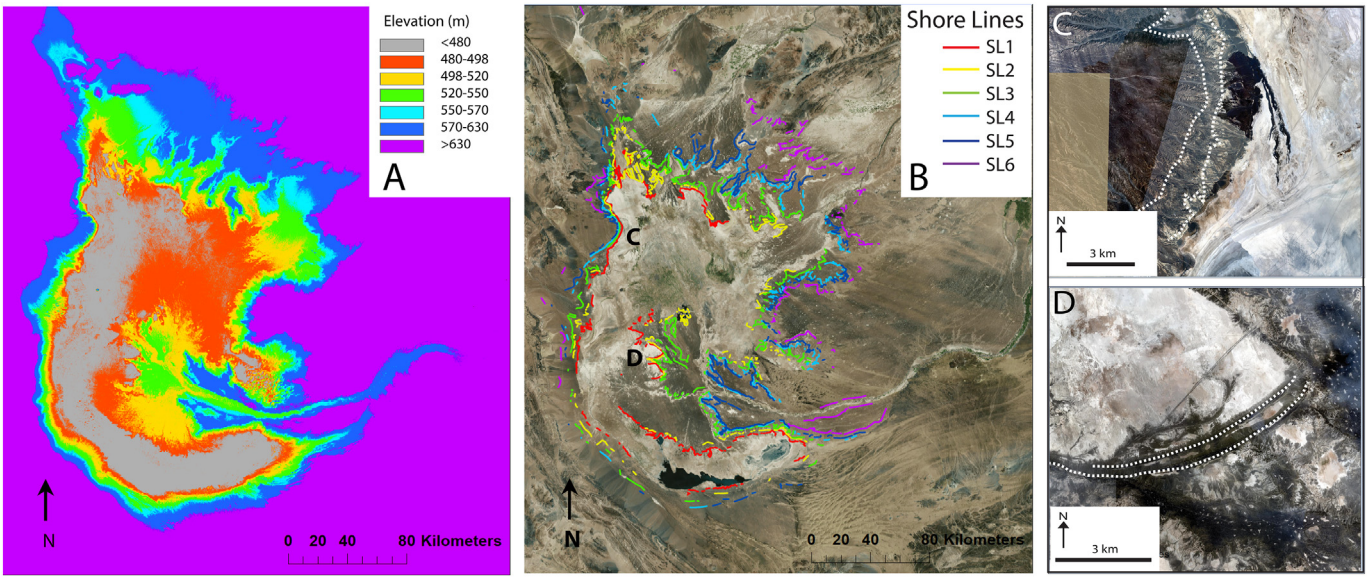

Fig. 6. (A) SRTM DEM of the Sistan Depression showing different colours for the different elevations of the shorelines (purple down to grey). (B) Shaded relief map of the Sistan Depression with former shorelines mapped. Locations of (C) and (D) to show close-up shorelines. (C) SPOT images of alluvial fan with wave cut platforms highlighted by white limestone layers (shown as white dashed lines). (D) SPOT images of beach ridge shorelines (shown as white dashed lines). (For interpretation of the references to colour in this figure legend, the reader is referred to the web version of this article.)

increases to 0.08° toward the foothills of the Hazarajat Mountains. The top of the plateau surface is fairly tabular (Fig. 3). Prominent erosional embayed scarps up to 200 m high mark the western edge of the plateau with the Sistan Depression (Fig. 3). The center of the Dasht-i Margo is incised by up to ~150 m by a relict fluvial system, the Dor Rud (Fig. 1B), which is now partly infilled by aeolian dunes. Numerous inverted channels, reaching up to 80 km in length, are prominent across the surface of the plateau. These inverted channels, which are likely partly cemented by carbonate (Smith, 1974; Doebrich et al., 2006), are particularly well developed along the edges of the plateau on the north and west sides where the regions between the channels are more eroded (Fig. 8). In these areas, the inverted channels form sinuous ribbons with heights up to ~20 m and range in width from 30 to 2000 m. The channel edges are consistently asymmetrical with steeper sides on the northwest and shallower sides on the southeast, consistent with wind erosion by the prevailing northwesterly winds. A series of sand bowls form where the inverted channels intersect and are later eroded out by wind erosion leaving small basins infilled with minor aeolian dunes or playas (Fig. 8). The inverted channels show a generally linear rather than bifurcating pattern away from the Hazaraket Mountains (Fig. 9).

5.2. Fluvial terraces

River terraces form from fluvial incision into older floodplain or channel sediments (Stokes et al., 2012). The terraces are usually preserved along the valley sides and represent the location of the former river channel system (Stokes et al., 2012). They have been used in numerous studies to reconstruct regional changes in climate and tectonics (e.g., Demir et al., 2004; Bridgland and Westaway, 2008; Walker and Fattahi, 2011; Bridgland et al., 2012; van Gorp et al., 2013).

A series of 11 staircase terraces was recognized along the edge of the Helmand Basin cutting into the northeastern side of the Dasht-i Margo Plateau (Figs. 3, 4, and 9). We interpret these terraces as being predominantly erosional. The texture between the terrace in shaded relief generated from ALOS data and satellite imagery images (from Landsat and TerraColor) shows no distinct change between the different terraces consistent with cutting into the same lithology (Fig. 4). Observations of paleochannel structures on the surface of many terraces indicate only minor sediment infilling has occurred once the new river level has been established, as is the case for the modern terrace-bound Helmand River.

The terraces are confined to the northeastern side of the Helmand River (Fig. 3). No equivalent terraces are observed on the southeast side of the river. Between the Koh-i-Khannesin volcano and the city of Lashkar Gah where the river valley is widest, 11 different terraces (T1–T11) are identified (Figs. 3 and 9). At cross section A–A′ (Fig. 9) the terraces vary in height between 24 and 114 m above the river floor (Fig. 9). The highest terrace (T11) shows the greatest width of 20 km, with the majority of the terraces below having widths between 5 and 4 km. Terraces T4 and T2 are the narrowest with 1.4 and 2.7 km widths respectively. Terraces T2 and T5 show isolated islands of the preceding terraces within the lower terraces (Fig. 9). Terraces T11 to T9 show wide aggradational deposition with a series of inverted channels preserved along their top surface, whereas terraces T8 to T1 show a more classic entrenched river terrace sequence (Fig. 4). The vertical height of the terraces varies from 4 to 15 m in terraces T11 to T2. Terrace T1 has a height of 24 m above the modern river channel. Upstream of cross section A–A′, the Arghandab River joins the Helmand River (Fig. 1), and the spatial relationship of the terraces becomes unclear. Across the Helmand region, T11 to T9 gradually curve from SSE-NNE to E-W (Fig. 9). Terraces T8 to T1 are deflected around the edge of the Koh-i Khannesin volcano (Figs. 4 and 9). Around the volcano, terraces T2-T6 and T8 are more restricted and curve round the volcano and then pinch out. As the valley widens on the western side of the volcano, several of the terraces reappear as well as a distinctive gravel terrace termed T9a (Fig. 9). Terraces T9a to T7 fan out toward the south, while terraces T4 to T1 are confined along the edges (within an 8-km zone) of the Helmand River. Terrace T5 is mapped a further 70 km to the west along the banks of the Helmand River from the Koh-i Khannesin volcano and terraces T1 and T2 for a further 160 km (Fig. 3B).

5.3. Delta systems

Several delta systems that terminate in the Sistan Depression have been recognized in the modern day and in geological records of the Helmand region (Whitney, 2006; Hartley et al., 2010). These systems are defined as megafans (apex to toe measuring 36 to 102 km) with low angle slopes (<0.05°) and a radial depositional pattern (Fig. 3). A series of seven distinct delta systems have been mapped fanning out into the Sistan Depression and termed D1–D7 from lowest to highest elevation (Fig. 5). The deltas can be seen fanning out from apex points that are marked A–D in Fig. 5.

The oldest mapped surface of D7 is preserved along both sides of the Helmand River (Fig. 5). On the southern side, the surface runs for 70 km and varies in elevation from 680 to 550 m (Figs. 5 and 7). The surface is less well preserved on the northern side, with the partly eroded sections infilled with aeolian deposits. The D7 surface on the southern side of the river shows several inverted channels exhumed along the edges of the deposits. The surface fans out from location A (Fig. 5) in a southwest direction with a slope of 0.03°.

Two of the highest elevation older delta systems (D5 and D6) correlate with the previously recorded delta, the Chahar Burjak (Fig. 1B). Deltas D6 and D5 fan out from the apex at location B (Fig. 5). The older of the two, D6, forms a small mesa (~100 km^2) on the north side of the Helmand River. The surface fans out with a slope of 0.04° to the northwest and varies in elevation from 640 to 630 m (Fig. 7). The younger delta, D5, runs on either side of the Helmand River for 50 km, sloping at 0.04° to the northeast. The fan forms a plateau, which varies in elevation from 600 to 560 m and shows a number of exhumed inverted channels along the edge of the deposit.

The next three younger delta systems (D4 to D2) fan out radially from point C (Fig. 5). Delta D4 shows the lowest preservation of these systems and is preserved as a series of three isolated units now forming a fan with a length of 50 km from toe to apex (Fig. 5). Delta D3 shows a slightly wider distributary pattern from southwest to north with a toe to apex length of 65 km and slope of 0.04°. The D2 shows the largest area of the delta system of over 2000 km^2 showing radial distribution toward the west (Fig. 5B). The youngest delta system, D1, represents the modern fluvial systems (Hartley et al., 2010) that fan out from point D (Fig. 5B) toward the north with a slope of 0.02°.

In summary, the delta systems migrate (telescope) in a western direction (locations A to C) and then shift to the north (location D). They decrease in elevation and vary in depositional direction from initially southwest to northwest (D7–5) to bimodal deposition to the north and south (D4–D2) until the modern system, which is predominantly to the north (D1).

5.4. Paleoshorelines

Former shorelines have previously been recognized within the Helmand Basin, 3 and 10 m above the present-day lake levels (Huntington, 1905). In our study six former lake shorelines have been recognized and mapped across the Helmand Basin at 8, 26, 48, 78, 98 and 158 m above the modern lake level (~472 m) (Fig. 6 and Table 1). The lowest shoreline (8 m) possible corresponds to the 10-m shoreline mentioned by Huntington (1905); however, the lower surface documented by Huntington of 3 m was not recognized from remote sensing imagery. The former shorelines have been termed SL 1–6 from lowest to highest. The preservation of the shorelines varies across the region, with several locations around the basin showing several additional shorelines (particularly in the south of the Helmand Basin), which could not be traced laterally across the area. The

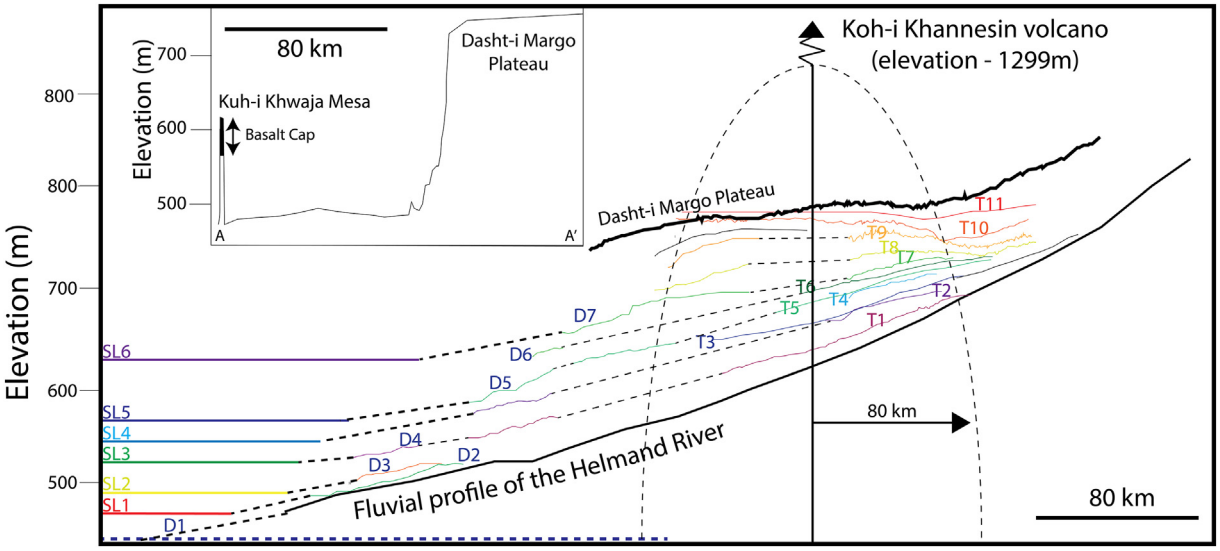

Fig. 7. Longitudinal profiles of the Helmand Region from SRTM DEM data. Location of elevation profiles shown in Fig. 3B as white lines. Solid black line shows the Dasht-i Margo Plateau. Spectrum of colours shows profiles taken from river terraces (T), delta systems (D), and lake shorelines (SL). Solid colour lines show exact elevations of profiles. Dotted lines show inferred contacts between profiles. Thin black line shows the modern Helmand River fluvial profiles. Vertical black line denotes the location of Koh-i Khannesin volcano and dashed curved black line is ca. 80 km radius from the volcano showing the upwarping of the terraces around the volcano.

northeastern side of the basin showed well preserved white beach deposits (Fig. 6C), while the northern part of the basin clearly showed wave cut platforms within the alluvial fans (Fig. 6D). The shorelines are also recognized adjacent to the base of the erosive scarps of the Dasht-i Margo Plateau (Fig. 6B). Several of the former shorelines, when traced around the delta systems, can be correlated with the deltas and terraces (Fig. 7). The shorelines are at the same elevation throughout the Helmand Basin (Table 1) indicating that no significant tectonic tilting has affected the western part of the Basin since they formed. The shorelines demark the history of the Sistan paleolake whose area has decreased from 50,800 km^2 to the modern 4000 km^2 (Table 1). Together the shorelines and correlated deltas define river base levels.

5.5. Longitudinal profile

All the features of the basin were combined to create a geomorphic map of the Helmand Basin (Fig. 3B). Longitudinal profiles of the plateau, terraces, deltas, and former shorelines were constructed along the Helmand River (Figs. 3 and 7). The location of the Koh-i Khannesin volcano has also been added as a reference. The terraces and deltas were correlated through mapping using remote sensing images (TerraColor and SPOT) and elevation profiles (SRTM DEM) across the region (Fig. 3). The former shorelines were combined with the deltas and terraces along the Helmand River. We also made correlations using a combination of elevation and cross-cutting relationships with some of the shorelines present on the upper delta systems and absent on the lower deltas. These observations were combined with the longitudinal profiles of the plateau, river terraces, deltas, and the former shorelines.

The plateau and terraces T11–T8 are only preserved as terraces and cannot be traced through to the delta system or former shorelines. Terrace T7 can be correlated along the Helmand River to D7 (Chahar Burjak) and shoreline 6 (158 m). Terrace T6 can be linked through to delta D6 but could not be correlated with a former shoreline. Terrace T5 is correlated with D5 and former shoreline 5 (98 m). Terrace T4 can only be found to the northeast of the Koh-i Khannesin volcano and cannot be correlated to any geomorphic surface to the southeast of the volcano. Terrace T3 can be linked through to a terrace running through the delta systems and linking to former shoreline 4 (78 m). Terrace T2 can only be recorded within 40 km of the Koh-i Khannesin

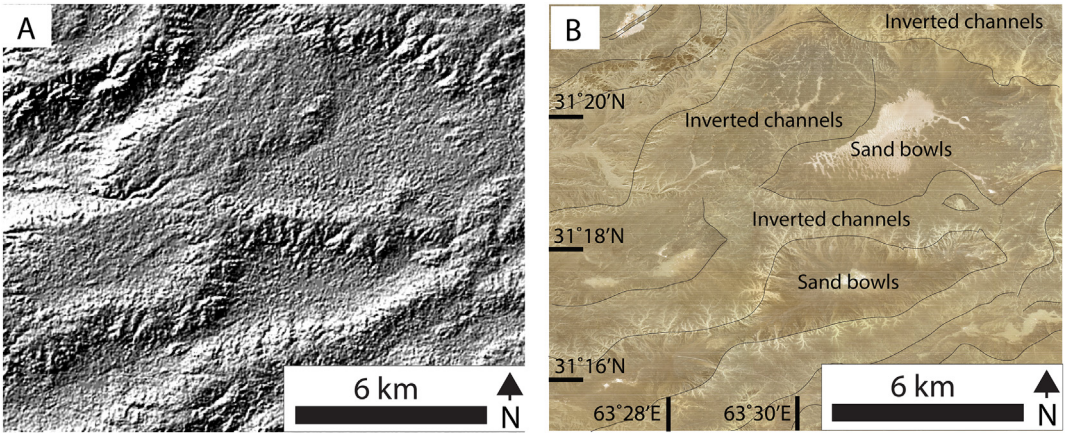

Fig. 8. Inverted channels preserved on the Dasht-i Margo Plateau. Location shown in Fig. 3B. (A) Shaded relief map of the channels constructed from ALOS data. (B) Satellite Pour l'Observation de la Terre (SPOT) satellite image of the same area with inverted channels and sand bowls marked.

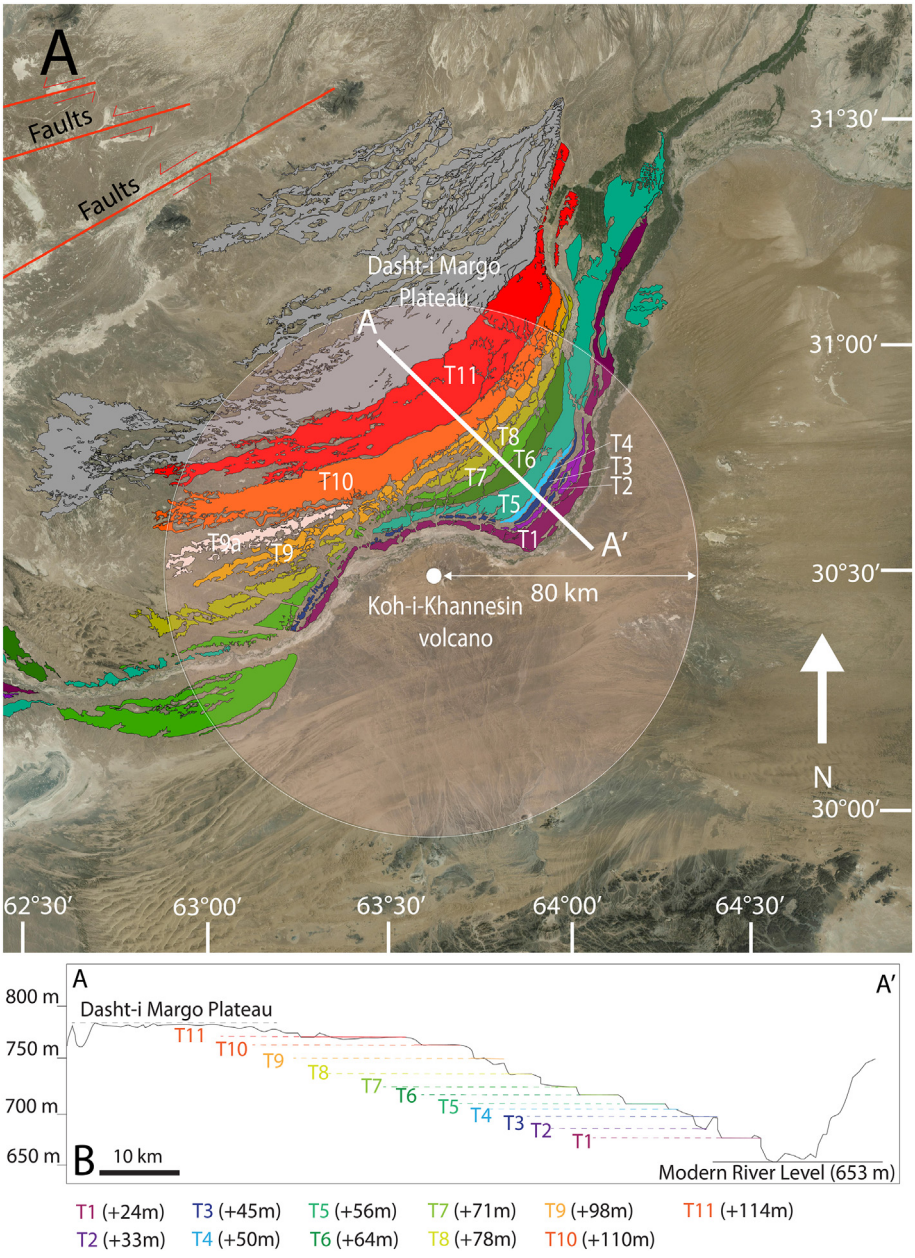

Fig. 9. (A) TerraColor image of the Helmand River with terraces (full spectrum of colours) mapped using methods discussed in the text and shown in Fig. 4. Faults mapped by Ruleman et al. (2007). (B) Cross section through the Dasht-i Margo Plateau, and staircase of terraces (T1 to T11) with elevations above the modern Helmand River quoted with accuracies of 5 m.

volcano. Terrace T1 is the most widely preserved terrace along the Helmand River and correlates through to the delta D4 and former shoreline 3 (48 m). The younger two delta systems (D2 and D3) show no clear link with terraces farther up the Helmand River but can be correlated with SL1 and SL2.

The longitudinal profiles of the geomorphic surface show two clear patterns on river profiles (Fig. 7). All the plateau, terraces, and distributary fluvial systems show a divergence of the profiles downstream, from the Hazaraket Mountains toward the Sistan Depression. The second pattern is proximal to the Koh-i Khannesin volcano; the plateau and terraces T11 to T7 show a convex upwarping, with an 80-km radius away from the volcano (Fig. 7). The minor drainage cutting into the plateau and terraces highlights this 80 km north of the volcano, as does the increase in erosion of the inverted channels 80 km to the northwest (Fig. 9). The higher terraces show a decrease in upwarping farther to the northwest.

6. Discussion

Our observations of the geologically recent landscape evolution of the Helmand Basin are based largely on remote sensing augmented by sparse geological data largely collected in the 1970s or before. With acute security issues becoming an increasing feature of many countries, such an approach may become common. The major factors influencing the long-term evolution of the Helmand Basin are tectonics and climate, a topic that has been long debated (Whitney, 2006, and references therein).

With regard to tectonics, the basin is likely enclosed because of the complex and ongoing interactions of regional plates. To the north the Hazarajat Mountains are the source for much of the sediment entering the basin through the contemporary Helmand River system and the earlier fluvial systems that make up the upper parts of the Dasht-i Margo Plateau. To the east, the active Chaman fault is accommodating much of the northward movement of India as it collides with the Asian plate to form

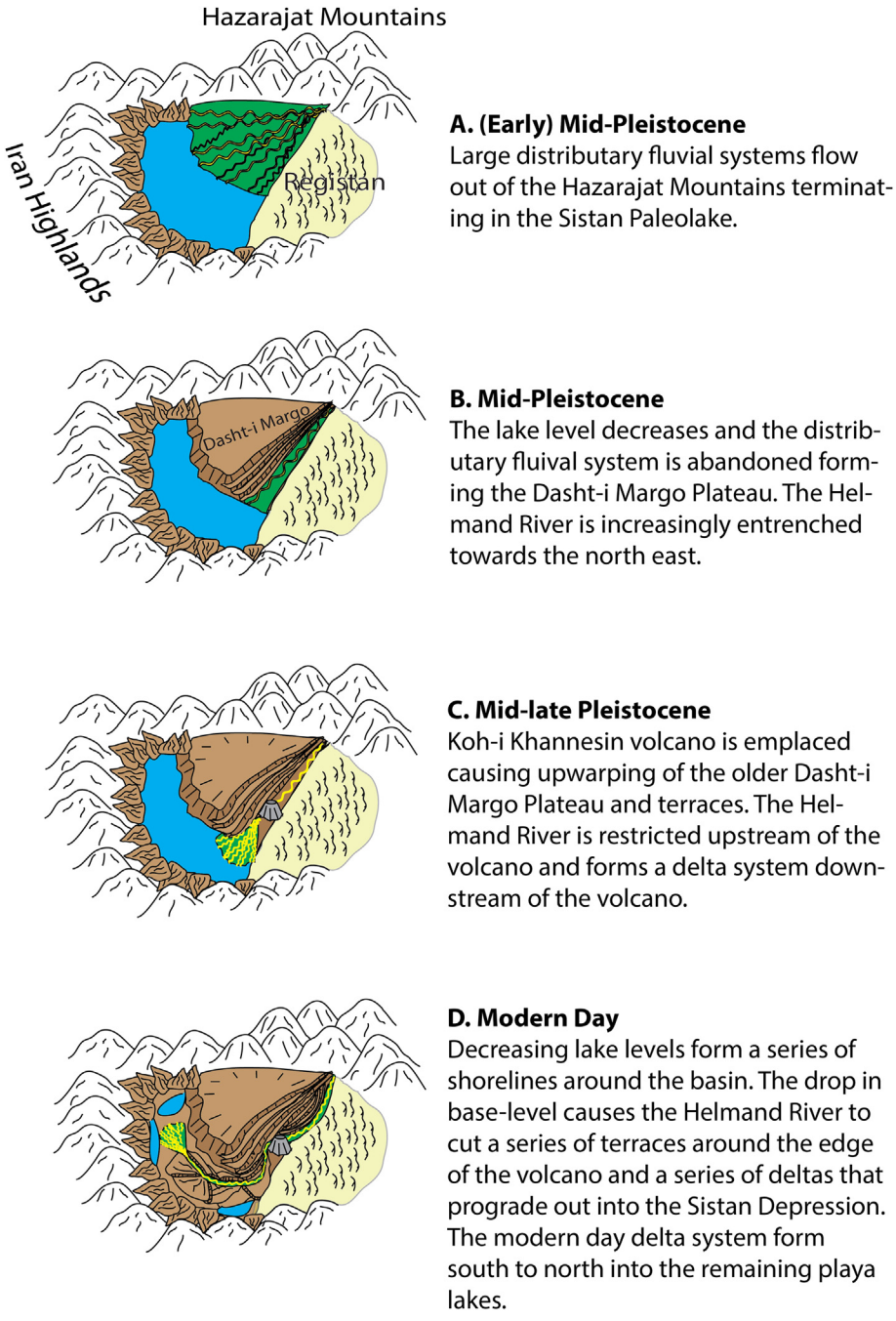
Hazarajat Mountains
Iran Highlands
Registan
A. (Early) Mid-Pleistocene
Large distributary fluvial systems flow out of the Hazarajat Mountains terminating in the Sistan Paleolake.
Dasht-i Margo
B. Mid-Pleistocene
The lake level decreases and the distributary fluival system is abandoned forming the Dasht-i Margo Plateau. The Helmand River is increasingly entrenched towards the north east.
C. Mid-late Pleistocene
Koh-i Khannesin volcano is emplaced causing upwarping of the older Dasht-i Margo Plateau and terraces. The Helmand River is restricted upstream of the volcano and forms a delta system downstream of the volcano.
D. Modern Day
Decreasing lake levels form a series of shorelines around the basin. The drop in base-level causes the Helmand River to cut a series of terraces around the edge of the volcano and a series of deltas that prograde out into the Sistan Depression. The modern day delta system form south to north into the remaining playa lakes.

Fig. 10. Paleogeographical reconstruction of the landscape evolution of the Helmand Basin.

the Himalayas. To the west, the eastern Iranian mountains are seismically active and part of a distributed zone of deformation across Iran related to the NNE movement of the Arabian plate. South of the basin, the Makran subduction zone is associated with a complex east-west compressional zone in Pakistan. However, our focus here is on the geological youthful system of terraces, deltas, and shorelines that we have documented. The observation that the paleolake shorelines have the same elevation around the Sistan Depression and that no major faults are observed to cut these features indicates no major deformation. We will return to the question of tectonics after presenting our interpretative history.

6.1. Landscape evolution of the Helmand Basin

The Dasht-i Margo Plateau is formed from the earliest fluvial system considered here (mapped in grey in Fig. 3B). This surface is characterised by preservation of inverted sinuous channels sourced from the Hazaraket Mountains to the northeast and feeding into the Sistan Depression to the west (Fig. 10A). The size of this system is comparable to some of Earth's larger distributary fluvial systems in drylands regions, such as the Warrego River, Australia, and the Batha River, Chad (Hartley et al., 2010). The inverted sinuous channels and absence of bifurcation suggest that the planform type was either multiple sinuous or single sinuous when active, which is consistent with the low angle of deposition and suggests a fairly low or continuous discharge with a low sediment supply (Hartley et al., 2010). This distributary fluvial system formed the upper coarse-grained gravels recorded at the top of the sedimentary sequence (Smith, 1974).

The marked drop in elevation (~200 m) at the edge of the plateau into the Sistan Depression indicates preferential erosion within the Sistan region that has cut back into the Dasht-i Margo Plateau through

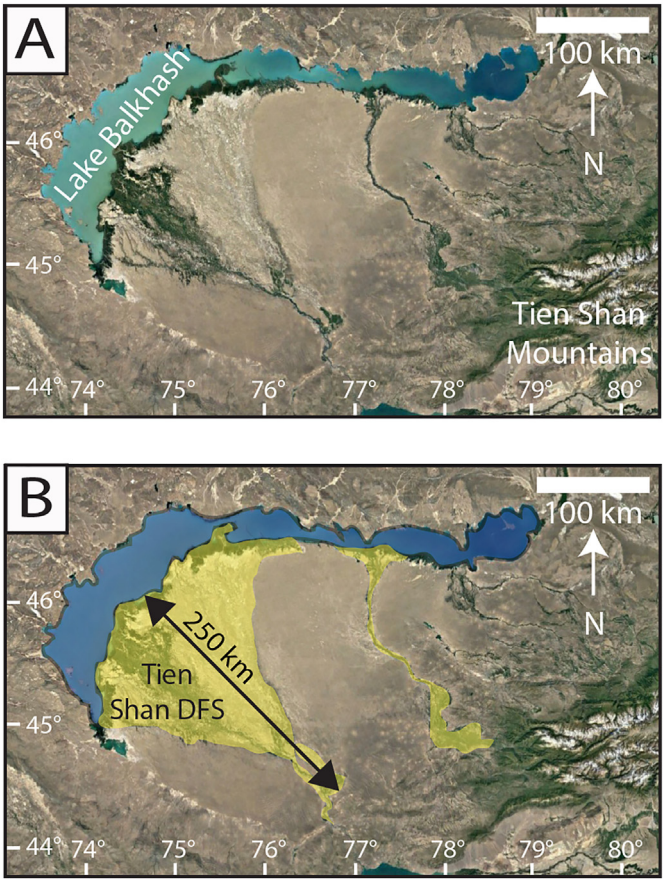

Fig. 11. Google Earth images of the Tien Shan region in east Kazakhstan. (A) Google Earth image of Tien Shan Mountains and Lake Balkhash. (B) Mapped distributary fluvial system (DFS) prograding NW from the Himalayan-Tibetan orogen, forming a 23,000 km^2 DFS with a toe-apex length of 260 km and terminating in Lake Balkhash. The fluvial system and lake are of a similar size and depositional style to that proposed for the Helmand Basin region.

time. The erosive scraps at the edge of the western plateau adjacent to the Sistan Depression must have formed before the formation of shoreline 6. A likely scenario is that the distributary fluvial system terminated into a large lake within the Sistan Depression (Fig. 10A). Assuming the western edge of the plateau marks the maximum edge of the lake, it would have been of a similar size as shown by shoreline 6 (>50,000 km^2). The lacustrine deposits from this lake, of unknown depth, that are lithologically weaker would have preferentially eroded within the Sistan Depression and eventually started to cut back into the Dasht-i Margo. The erosive agent is attributed to the desert winds that would have removed the fine-grained lacustrine sediments and deposited them within the Registan region as the extensive dune field, which is in keeping with the modern studies (Ranjbar and Iranmanesh, 2008; Hamzeh et al., 2016) (Fig. 2). The high erosivity of the desert wind is evident from yardangs, dune fields, and asymmetric development of the inverted channels (Whitney, 2006) and is supported by the lacustrine sediment preserved below the Kuh-I Khwaja mesa (Fig. 3) (105 m high) in the Sistan Depression. This observation indicates a previously much larger lake than is currently within the region. A modern-day example of a system of this size would be the Tien Shan region within Kazakhstan, which hosts a large distributary fluvial system (area: 23,000 km^2, apex to toe 260 km) forming off the active Tien Shan Mountain range terminating into Lake Balkhash (17,000 km^2) (Fig. 11).

The next stage in the evolution of the area was the formation of the earlier terraces (T11 to T8) as the Dasht-i Margo Plateau was abandoned (Fig. 10B). The axis of the paleo Helmand fluvial system migrated to the east and progressively narrowed (Fig. 10B). The terracing indicates the start of an episodic process characterised by alternation of downcutting through earlier fluvial sediments and into the older sediments (the lower unit of Smith, 1974) of the Dasht-i Margo Plateau and then stabilisation. These successive fluvial systems supplied sediment into the Sistan Depression formed by the earlier late-Miocene-Pliocene erosional episode.

The influence of the Koh-i Khannesin Volcano on the terrace morphology is significant to constrain the ages. The course of the rivers associated with terraces T11 to T8 are not influenced by the volcano, but terraces T7 to T1 are deflected around the volcano (Fig. 3). However, the Dasht-i Margo Plateau and terraces T11 to T8 are upwarped in the vicinity of the volcano (Fig. 7) over a region of at least 80 km, while T7 to T1 are not upwarped (Fig. 10C). Long wavelength topography created by magma emplacement has been well documented in the Andes with similar wavelength that are documented here (e.g., Froger et al., 2007; Perkins et al., 2016). These observations suggest that the volcano largely formed in the time between T8 and T7 (Fig. 10C). The only date for the volcano is 0.61 ± 0.05 Ma, however, below we develop an interpretation of episodic terrace formation as a consequence of Milankovitch climate cycles, which is consistent with an age of around 0.6 Ma for T7. The approximate age of T7 indicates that terraces T11 to T8 formed in the early to mid-Pleistocene, while terraces T6-T2 formed in the late Pleistocene.

Terraces T6 to T1 record further systematic narrowing and migration of the Helmand River system to the east and south (Figs. 3 and 10D). These terraces can be correlated with delta systems entering into the Sistan Basin. These fans migrate to the west and then north with time, and each delta fan is partly cut by the rivers related to younger delta (Fig. 10D). The terraces and deltas can be correlated with the six shorelines showing the presence of a large lake that has, since SL6 times, had undergone a marked reduction in volume. The area of the lake in SL6 times was >50,000 km^2. We interpret these changes in terms of tectonics and climate change as developed in the next sections.

6.2. Cause of base-level changes

The simplest explanation of the downcutting of the Helmand River into the Dasht-i Margo plateau is a change in base level. Subsidence of the Sistan Basin is a possibility, but the lack of any deformation of the shorelines makes this an unlikely explanation especially for the time period of T7 to T1 formation. Uplift of the tectonically active Helmand block in the northeast corner of the basin, which is the source of the Helmand River, could be another cause of base-level change. The Helmand block is a region of active erosion bound by major SW-NE trending faults and containing numerous smaller faults with some contemporary seismicity and exposure of Cretaceous rocks (Wheeler et al., 2005; Shiel, 2017). However, the longitudinal fluvial profiles show a divergence toward the base level suggesting that it is the main controlling factor. As such, a decrease in the elevation, depth, and area of the Sistan paleolake is the simplest explanation of the change of base level for terraces T7 to T1; with no requirement to invoke tectonic effects.

Less clear is why the river system progressively migrated to the east and south. The plateau may have experienced minor tilting to the

Table 1
Lake shoreline elevations, meters above modern lake levels, and surface area estimates.

Lake line	Elevation (m.s.l.)	Meters above modern lake level (m)	Surface area (km^2)
Modern	472	0	4000
Shoreline 1	480	8	12,800
Shoreline 2	498	26	20,300
Shoreline 3	520	48	27,400
Shoreline 4	550	78	34,000
Shoreline 5	570	98	37,700
Shoreline 6	630	158	50,800

southeast, perhaps related to the Farah fault on the northwest side of the plateau. The high >500-m elevation of the Registan region above the present-day Helmand River and 300 m above the Dasht-i Margo Plateau confined the fluvial system along the southeastern margin.

6.3. Climate controls

The well-preserved staircase terraces cutting down into the Dasht-i Margo Plateau suggest that periods of fluvial incision were interspersed with long periods of stability allowing a wide fluvial system to develop. These systems were then abandoned because of a rapid decrease in the fluvial profile, leaving the older system behind as a raised terrace along the edge of the river. Likewise, the formation of discrete shorelines and delta systems that can be correlated with the terraces indicate strongly episodic processes involving regular cyclic changes in discharge, lake level, and sediment supply. We attribute this episodicity to global Milankovitch glacial-interglacial cycles. We have identified 11 terraces. The Past Interglacials Working Group of PAGES (2016) has identified 11 interglacial periods in the last 800,000 years. The fourth oldest of these cycles is at ~600 ky, which is close to the age of T7 terrace which is the first terrace to be influenced by the Koh-i Khannesin volcano dated at 610 ky. Likewise the fluvial terrace shift in style from wide distributary aggradation sheets (plateau to T9) to more steeply entrenched terraces (T8–T1) is in the mid-Pleistocene. This correlates with a global shift in fluvial terrace sequences that is attributed to the Mid-Pleistocene Revolution (Bridgland and Westaway, 2008) related to the transition between weaker cycles with a period of about 40 ka and much stronger cycles closer to 100 ka (Past Interglacials Working Group of PAGES, 2016). These same cycles may link through to 10 pluvial to arid phases based on alternating oxic to anoxic lacustrine sediments recorded in the Sistan Depression (Huntington, 1905).

The Helmand River accounts for 80% of the fluvial discharge into the basin and is largely supplied by snow and glacier meltwaters from the catchment area in the Hazarajat Mountains. During glacial to interglacial periods, changes in the climate within the catchment area leads to a rapid response of fluvial systems within the basin (Cordier et al., 2017). The western Himalayas is affected by Milankovitch Cycles that control the strength of the Siberian High and the Mid-Latitude Westerlies (Owen and Dortch, 2014). During glacial periods, the increase in precipitation expands glaciers and increases precipitation (as snow); while during the shift from glacial to interglacial the water stored as ice is released, increasing the fluvial discharge and sediment supply, resulting in increased erosion and downcutting in the basin (Cordier et al., 2017). The onset of shorter interglacial periods is also associated with a drier warmer climate and a drop in lake elevation, resulting in the river base level dropping and leading to downcutting and terrace formation.

The Sistan paleolake reached its greatest volume from the late to mid-Pleistocene. The climate was significantly wetter then and has dried out since. This history is similar to the Lut Desert, eastern Iran, that has also shown drying out during the Pleistocene (Bobek, 1969; Krinsley, 1970; Dresch, 1976).

Within the Holocene the climate has also switched between arid to more humid conditions but on a smaller scale (Hamzeh et al., 2016). The youngest two distributary fluvial systems (D3 and D2) and shorelines (SL1 and SL2) suggest much smaller changes that only affect the lower part of the fluvial network since the last glaciation period. These fluctuations in climate of D3 and SL2 may correspond to shifts in the climate recorded at 60–40 ka by incision of fluvial networks into older alluvial fans in eastern Iran (Fattahi et al., 2006). The younger D2 and SL1 most likely link to an increase in lake size from 6 to 3.8 ky, correlating with the Bronze Age settlements along the edge of distributary fluvial system D2 and paleoshoreline 1, with abandonment of the settlement post-3.8 ky linked with a decrease in lake size to modern day levels (Hamzeh et al., 2016).

7. Conclusions

Detailed analysis of remotely sensed data and sparse geological data from the Helmand Basin has provided new insights into the Quaternary evolution of the region summarised as follows.

- The Helmand Basin has had a long history of sedimentation derived from uplift of the Hindu Kush-Karakoram Himalayan Mountains. A period of erosion of these sediments and related volcanics occurred in the late Miocene and Pliocene, creating erosional remnants and scraps up to 200 m high of the Dasht-i Margo Plateau that bounds the eastern side of the Sistan Depression.
- A large low-relief distributary fluvial system sourced from the Hazaraket Mountains initially formed across the surface of the Dasht-i Margo Plateau in the early Pleistocene.
- Incision of the Dasht-i Margo Plateau of up to 180 m initiated along its eastern and southern margins, and the distributary fluvial system was abandoned. A succession of 11 terraces (T1 to T11) is recognized cutting into the plateau. The terraces record narrowing and migration of the paleo-Helmand river to the east and increasing incision into the plateau. Nine of the terraces can be correlated over distances >80 km to reconstruct paleolongitudinal fluvial profiles.
- The younger terraces (T1 to T7) can be correlated with paleolake shorelines (SL1 to SL6) and seven delta systems (D1 to D7) in the Sistan Depression. These features record a decrease in lake volume and drop in river base level.
- The upper 5 profiles (T11-T8) show upwarping over a distance of 80 km around the Koh-i Khannesin volcano. The profiles suggest that these terraces developed prior to growth of the volcano at ca. 0.61 Ma, while later terraces (T6–T1) formed after the volcano was established.
- We correlate the terraces with the 11 major glacial-interglacial Milankovitch cycles in the last 800 ka.
- Drying out of the region since the mid-Pleistocene has led to a restricted fluvial input of the Helmand River and gradual base level drop in the Sistan Depression, with fluvial incision into the Dasht-i Margo Plateau as a consequence.
- Seven main delta systems within the Helmand Basin flow into the Sistan Depression and show a progradation from oldest in the east to youngest in the west. Only the modern delta system is confined to the northern edge of the Sistan Depression.
- Six former lake shorelines are recognized within the Sistan Depression with heights of 8, 26, 48, 78, 98 and 158 m above the modern lake level (~472 m). These shorelines can be traced throughout the Sistan Depression at consistent elevations, suggesting no tectonic tilting since they were formed.
- The longitudinal profiles of the Dasht-i Margo Plateau and Helmand River terraces combined with the delta systems and former shorelines suggest a pulsed drying of the Helmand Basin since the mid-Pleistocene, most likely linked with global glacial and interglacial periods that can be correlated with similar climate changes within Iran and the western Himalayas.

Supplementary data to this article can be found online at https://doi.org/10.1016/j.geomorph.2018.03.018.

Acknowledgements

This study was funded by a University of Bristol Cabot Institute Innovation Award to Laura Evenstar. This manuscript was greatly improved by reviews from Martin Stoke, University of Plymouth, and two anonymous reviewers. This manuscript would not have been possible without workspace by Theatro.

References

Aitchison, J.C., Ali, J.R., Davis, A.M., 2007. When and where did India and Asia collide? J. Geophys. Res. Solid Earth 112.

Atwood, G., 1994. Geomorphology applied to flooding problems of closed-basin lakes specifically Great Salt Lake, Utah. Geomorphology 10, 197–219.

Bachofer, F., Quénéhervé, G., Märker, M., 2014. The delineation of paleo-shorelines in the Lake Manyara basin using TerraSAR-X data. Remote Sens. 6, 2195–2212.
Benn, D.I., Owen, L.A., 1998. The role of the Indian summer monsoon and the mid-latitude westerlies in Himalayan glaciation: review and speculative discussion. J. Geol. Soc. Lond. 155, 353–363.
Bobek, H., 1969. Zur Kenntnis der südlichen Lut. Mitteilungen der Österreichischen Geographischen Gesellschaft 111, pp. 155–192.
Bridgland, D., Westaway, R., 2008. Climatically controlled river terrace staircases: a world-wide Quaternary phenomenon. Geomorphology 98, 285–315.
Bridgland, D.R., Westaway, R., Romieh, M.A., Candy, I., Daoud, M., Demir, T., Galiatsatos, N., Schreve, D.C., Seyrek, A., Shaw, A.D., 2012. The River Orontes in Syria and Turkey: downstream variation of fluvial archives in different crustal blocks. Geomorphology 165, 25–49.
Casanova, J., Hillaire-Marcel, C., 1992. Chronology and paleohydrology of late Quaternary high lake levels in the Manyara Basin (Tanzania) from isotopic data (^{18}O, ^{13}C, ^{14}C, ThU) on fossil stromatolites. Quat. Res. 38, 205–226.
Clapperton, C., 1993. Quaternary Geology and Geomorphology of South America.
Cooper, F.J., Adams, B.A., Edwards, C.S., Hodges, K.V., 2012. Large normal-sense displacement on the South Tibetan fault system in the eastern Himalaya. Geology 40, 971–974.
Cordier, S., Adamson, K., Delmas, M., Calvet, M., Harmand, D., 2017. Of ice and water: quaternary fluvial response to glacial forcing. Quat. Sci. Rev. 166, 57–73.
Currey, D.R., 1990. Quaternary palaeolakes in the evolution of semidesert basins, with special emphasis on Lake Bonneville and the Great Basin, USA. Palaeogeogr. Palaeoclimatol. Palaeoecol. 76, 189–214.
Demir, T., Yeşilnacar, İ., Westaway, R., 2004. River terrace sequences in Turkey: sources of evidence for lateral variations in regional uplift. Proc. Geol. Assoc. 115, 289–311.
DeVogel, S.B., Magee, J.W., Manley, W.F., Miller, G.H., 2004. A GIS-based reconstruction of late Quaternary paleohydrology: Lake Eyre, arid central Australia. Palaeogeogr. Palaeoclimatol. Palaeoecol. 204, 1–13.
Doebrich, J.L., Wahl, R.R., Chirico, P.G., Wandrey, C.J., Bohannon, R.G., Orris, G.J., Bliss, J.D., Wasy, A., Younusi, M.O., 2006. Geologic and Mineral Resource Map of Afghanistan (No. 2006-1038). Geological Survey, US.
Dortch, J.M., Owen, L.A., Caffee, M.W., 2013. Timing and climatic drivers for glaciation across semi-arid western Himalayan–Tibetan orogen. Quat. Sci. Rev. 78, 188–208.
Drake, N., Bristow, C., 2006. Shorelines in the Sahara: geomorphological evidence for an enhanced monsoon from palaeolake Megachad. The Holocene 16, 901–911.
Dresch, J., 1976. Bassins arides iraniens. Bulletin de l'Association de Géographes Français 430, pp. 337–351.
Fattahi, H., Amelung, F., 2016. InSAR observations of strain accumulation and fault creep along the Chaman Fault system, Pakistan and Afghanistan. Geophys. Res. Lett. 43, 8399–8406.
Fattahi, M., Walker, R., Hollingsworth, J., Bahroudi, A., Nazari, H., Talebian, M., Armitage, S., Stokes, S., 2006. Holocene slip-rate on the Sabzevar thrust fault, NE Iran, determined using optically stimulated luminescence (OSL). Earth Planet. Sci. Lett. 245, 673–684.
Froger, J.-L., Rémy, D., Bonvalot, S., Legrand, D., 2007. Two scales of inflation at Lastarria-Cordon del Azufre volcanic complex, central Andes, revealed from ASAR-ENVISAT interferometric data. Earth Planet. Sci. Lett. 255, 148–163.
Gaber, A., Ghoneim, E., Khalaf, F., El-Baz, F., 2009. Delineation of paleolakes in the Sinai Peninsula, Egypt, using remote sensing and GIS. J. Arid Environ. 73, 127–134.
Garcin, Y., Melnick, D., Strecker, M.R., Olago, D., Tiercelin, J.-J., 2012. East African mid-Holocene wet–dry transition recorded in palaeo-shorelines of Lake Turkana, northern Kenya Rift. Earth Planet. Sci. Lett. 331, 322–334.
Goes, B., Howarth, S., Wardlaw, R., Hancock, I., Parajuli, U., 2016. Integrated water resources management in an insecure river basin: a case study of Helmand River Basin, Afghanistan. Int. J. Water Resour. Dev. 32, 3–25.
Hamzeh, M.A., Gharaie, M.H.M., Lahijani, H.A.K., Djamali, M., Harami, R.M., Beni, A.N., 2016. Holocene hydrological changes in SE Iran, a key region between Indian summer monsoon and Mediterranean winter precipitation zones, as revealed from a lacustrine sequence from Lake Hamoun. Quat. Int. 408, 25–39.
Hartley, A.J., Weissmann, G.S., Nichols, G.J., Warwick, G.L., 2010. Large distributive fluvial systems: characteristics, distribution, and controls on development. J. Sediment. Res. 80, 167–183.
Horton, B., DeCelles, P., 2001. Modern and ancient fluvial megafans in the foreland basin system of the central Andes, southern Bolivia: implications for drainage network evolution in fold-thrust belts. Basin Res. 13, 43–63.
Huntington, E., 1905. The depression of Sistan in eastern Persia. Bull. Am. Geogr. Soc. 37, 271–281.
Jux, U., Kempf, E., 1983. Regional geology of Sistan (Southwest Afghanistan). Prehistoric Sistan 1, 5–60.
Kehl, M., 2009. Quaternary climate change in Iran—the state of knowledge. Erdkunde 1–17.
Krinsley, D.B., 1970. A Geomorphological and Paleoclimatological Study of the Playas of Iran. US Geological Survey, Washington, D.C.
Lavé, J., Avouac, J.-P., 2000. Active folding of fluvial terraces across the Siwaliks Hills, Himalayas of central Nepal. J. Geophys. Res. Solid Earth 105, 5735–5770.
Lu, Z., Kim, J.W., Lee, H., Shum, C.K., Duan, J., Ibaraki, M., Akyilmaz, O., Read, C.H., 2009. Helmand river hydrologic studies using ALOS PALSAR InSAR and ENVISAT altimetry. Mar. Geod. 32, 320–333.
McCauley, J., Grolier, M., Breed, C., 1977. Yardangs. Geomorphology in Arid Regions, pp. 233–269.
Owen, L.A., Dortch, J.M., 2014. Nature and timing of Quaternary glaciation in the Himalayan–Tibetan orogen. Quat. Sci. Rev. 88, 14–54.
Owen, L.A., Bailey, R.M., Rhodes, E.J., Mitchell, W.A., Coxon, P., 1997. Style and timing of glaciation in the Lahul Himalaya, northern India: a framework for reconstructing late Quaternary palaeoclimatic change in the western Himalayas. J. Quat. Sci. 12, 83–109.
Past Interglacials Working Group of PAGES, 2016. Interglacials of the last 800,000 years. Rev. Geophys. 54, 162–219.
Perelló, J., Razique, A., Schloderer, J., 2008. The Chagai porphyry copper belt, Baluchistan province, Pakistan. Econ. Geol. 103, 1583–1612.
Perkins, J.P., Finnegan, N.J., Henderson, S.T., Rittenour, T.M., 2016. Topographic constraints on magma accumulation below the actively uplifting Ututuncu and Lazufre volcanic centers in the Central Andes. Geosphere 12, 1078–1096.
Pias, J., 1972. Geological, pedological and paleoclimatic significance of Paleolacustrian and delta formations in Seistan (Southern Afghanistan). C. R. Hebd. Seances Acad. Sci. Ser. D 274, 1143–1148.
Pias, J., 1976. Formations superficielles et sols d'Afghanistan. IRD Editions.
Quittmeyer, R., Jacob, K., 1979. Historical and modern seismicity of Pakistan, Afghanistan, northwestern India, and southeastern Iran. Bull. Seismol. Soc. Am. 69, 773–823.
Ranjbar, M., Iranmanesh, F., 2008. Effects of Drought on Wind Eroding and Erosion in Sistan Region With Use of Satellite Multiple Images. Islamic Azad University, Shahre Rey Branch, pp. 14–30.
Reilinger, R., McClusky, S., 2011. Nubia–Arabia–Eurasia plate motions and the dynamics of Mediterranean and Middle East tectonics. Geophys. J. Int. 186, 971–979.
Ruleman, C., Crone, A., Machette, M., Haller, K., Rukstales, K., 2007. Map and Database of Probable and Possible Quaternary Faults in Afghanistan. Geological Survey, US.
Schreiber, A., Weippert, D., Wittekindt, H.-P., Wolfart, R., 1972. Geology and petroleum potentials of central and south Afghanistan. AAPG Bull. 56, 1494–1519.
Shiel, A., 2017. Structural setting and evolution of the Afghan orogenic segment – a review. Geol. Soc. Lond., Spec. Publ. 427, 57–88.
Smith, G.I., 1974. Quaternary deposits in southwestern Afghanistan. Quat. Res. 4, 39–52.
Stokes, M., Cunha, P.P., Martins, A.A., 2012. Techniques for analysing Late Cenozoic river terrace sequences. Geomorphology 165-166, 1–6.
Stokes, M., Mather, A., Belfoul, M., Faik, F., Bouzid, S., Geach, M., Cunha, P.P., Boulton, S., Thiel, C., 2017. Controls on dryland mountain landscape development along the NW Saharan desert margin: insights from Quaternary river terrace sequences (Dadès River, south-central High Atlas, Morocco). Quat. Sci. Rev. 166, 363–379.
Syvitski, J.P., Overeem, I., Brakenridge, G.R., Hannon, M., 2012. Floods, floodplains, delta plains—a satellite imaging approach. Sediment. Geol. 267, 1–14.
Ul-Hadi, S., Khan, S.D., Owen, L.A., Khan, A.S., 2013. Geomorphic response to an active transpressive regime: a case study along the Chaman strike-slip fault, western Pakistan. Earth Surf. Process. Landf. 38, 250–264.
van Gorp, W., Veldkamp, A., Temme, A., Maddy, D., Demir, T., van der Schriek, T., Reimann, T., Wallinga, J., Wijbrans, J., Schoorl, J., 2013. Fluvial response to Holocene volcanic damming and breaching in the Gediz and Geren rivers, western Turkey. Geomorphology 201, 430–448.
Walker, R.T., Fattahi, M., 2011. A framework of Holocene and Late Pleistocene environmental change in eastern Iran inferred from the dating of periods of alluvial fan abandonment, river terracing, and lake deposition. Quat. Sci. Rev. 30, 1256–1271.
Warsaw, 1984. National Atlas of the Democratic Republic of Afghanistan. Organization for Surveying & Cartography GEOKART.
Wheeler, R.L., Bufe, C.G., Johnson, M.L., Dart, R.L., Norton, G., 2005. Seismotectonic Map of Afghanistan, With Annotated Bibliography. US Department of the Interior, US Geological Survey.
Whitney, J.W., 2006. Geology, Water, and Wind in the Lower Helmand Basin, Southern Afghanistan.
Wittekindt, H., Weippert, D., 1973. Geologische Karte von Zentral und Süd-Afghanistan 1: 500 000: Geological map of central and southern Afghanistan. Bundesanstalt für Bodenforschung.